General Disclaimer

One or more of the Following Statements may affect this Document

- This document has been reproduced from the best copy furnished by the organizational source. It is being released in the interest of making available as much information as possible.

- This document may contain data, which exceeds the sheet parameters. It was furnished in this condition by the organizational source and is the best copy available.

- This document may contain tone-on-tone or color graphs, charts and/or pictures, which have been reproduced in black and white.

- This document is paginated as submitted by the original source.

- Portions of this document are not fully legible due to the historical nature of some of the material. However, it is the best reproduction available from the original submission.

FROM:

Space Physics Group
Department of Physics & Astronomy
University of Maryland
College Park, Maryland 20742
U.S.A.

TIME-OF-FLIGHT TECHNIQUE FOR PARTICLE IDENTIFICATION AT ENERGIES FROM 2 to 400 KEV/Nucleon

G. GLOECKLER*

Department of Physics and Astronomy, University of Maryland
College Park, MD 20742

and

K.C. HSIEH*

Department of Physics, University of Tucson
Tucson, AZ 85721

UNIVERSITY OF MARYLAND
DEPARTMENT OF PHYSICS AND ASTRONOMY
COLLEGE PARK, MARYLAND

TIME-OF-FLIGHT TECHNIQUE FOR PARTICLE IDENTIFICATION AT ENERGIES FROM 2 to 400 KEV/Nucleon

G. GLOECKLER*

Department of Physics and Astronomy, University of Maryland
College Park, MD 20742

and

K.C. HSIEH†

Department of Physics, University of Tucson
Tucson, AZ 85721

ABSTRACT

We have extended the time-of-flight technique for particle identification to 2 keV/nucleon and reduced the size of the start-time detector considerably by the use of carbon foils of few $\mu g/cm^2$ in thickness combined with microchannel plates for detecting secondary electrons. Time-of-flight telescopes incorporating this start-time device have been used to measure the stopping power of a number of low energy heavy ions in thin carbon foils and the charge states of these ions emerging from such foils. Applications of this technique for the detection and identification of low energy interplanetary and magnetospheric particles are suggested.

---

* Supported in part by NASA grant NGR 21-002-224 and NGR 21-002-316.

† Supported in part by NASA grant NGR 03-002-107.

1. INTRODUCTION

The use of the time-of-flight (TOF) technique for mass spectrometry in particle physics is well established[1]. To achieve a low energy response secondary electrons emitted off a thin foil (e.g. carbon) due to the passage of an ion have been used to provide the zero-time or START signal in TOF telescopes[2-4]. We have extended these techniques to the detection and identification of particles of energies as low as a few keV/nucleon by using carbon foils 2-3 $\mu g/cm^2$ in thickness in the START detector. In one case we have also simplified the STOP detector by having the ions incident directly on a microchannel plate (MCP). New results on the stopping power and straggling of low energy ions in carbon, and charge-state distribution of ions emerging from carbon foils have been obtained by this technique. Applications for the detection and identification of low energy charged and neutral particles in space are suggested.

2. INSTRUMENTATION

The two time-of-flight telescopes (TOF-I and TOF-II) used in this work are shown schematically in Fig 1a and 1b respectively. The secondary electron detector assembly (SEDA) for the START signal in both configurations consists of a thin carbon foil mounted over a $\sim 5mm^2$ circular opening of the SEDA front plate, a 95% transmission acceleration grid, a pair of chevron mounted microchannel plates (MCP), and a 50-Ω impedance-matched anode assembly[4]. Incident ions enter the carbon foil at 45^o with respect to the foil, and leave the START SEDA through an opening on its side. Secondary electrons which are emitted from the foil on the side of the exiting ions are accelerated to 1 KeV by the electric field between the foil and the acceleration grid and travel to the front of the MCP where they produce a $\lesssim 1$ ns rise-time, large amplitude START pulse at the anode. A typical pulse-height

distribution of the START signals for 25 kev H^+, He^+ and H_2^+ is shown in Fig 2a. For convenience the anode was operated at ground potential, the foil was biased at typically -3.7 kV, and across each of the MCPs a 1.1 KV potential was applied.

The STOP signals are generated differently in the two TOF configurations. While TOF-II uses a STOP SEDA identical to the START SEDA as shown in Fig 1b, the STOP signal in TOF-I is derived from a MCP which detects the ions directly. Pulse-height spectra of the TOF-I STOP signals are shown in Fig 2b. In TOF-II we use in addition a conventional surface-barrier Au-Si detector to measure the residual energy of the ions which have traversed the START and STOP SEDAs.

The block diagram of the electronics used for signal processing and recording of data was identical for both TOF configurations and is shown in Fig 3. The START and STOP pulses go to their respective constant-fraction discriminators (D), and then to the time-to-amplitude converter (TAC). For the STOP pulse a fixed (DL1) and variable (DL2) delay is introduced before the input to the TAC. By adjusting these delays one can calibrate the system and fully utilize the range of the TAC. The output of the TAC goes through a biased amplifier (BA) into a pulse-height analyzer (PHA). The pulse-height data, corresponding to the time lapse between the START and STOP signals is recorded on paper tape and plotted by means of an X-Y recorder for further analysis.

By taking the ratio of the coincidence counting rate of the START and STOP detectors to the singles counting rate of the STOP detector, the efficiency of the START detector was determined to be 90% at an incident ion rate of $10^2 sec^{-1}$. With TOF-I we also measured the delay time in the start signal to be 1.3 ± 0.5 ns, consistent with the expected travel time of the secondary electrons between the foil and the MCP of the START detector.

3. OBSERVATIONS

By exposing TOF-I and TOF-II to ion beams betewen 2-400 keV/nucleon, we obtained information on the intrinsic timing resolution of the telescopes, straggling and stopping power of low energy ions in carbon foils, and charge-state distributions of 10-50 keV H^+ and He^+ after traversing a thin carbon foil.

Intrinsic timing resolution and straggling: In Fig 4 we show the resolution in the time-of-flight measurement for various ions with incident energy of 25 keV. Although the resolution for the low mass ions is impressive, the relative uncertainties in the time-of-flight determination increases for heavier particles as may be seen in case of the CO^+ ions. The uncertainties in the TOF measurement result from a combination of systems noise (due to time-of-flight dispersion of secondary electrons and noise in the MCP and associated electronics) and the energy straggling of ions in the foil. However, only the latter depends on the type and energy of the incident particle. Fig 5 shows the timing uncertainty $\Delta\tau/\tau$ for different species as a function of incident particle energy. The quantity $\Delta\tau/\tau$, which is the ratio of the FWHM of the TOF pulse-height distribution to the average time-of-flight for a given ion species at a given energy, can be expressed as $\Delta\tau/\tau = \tau^{-1}\sqrt{(\Delta\tau_s)^2 + (\Delta\tau_e)^2}$, where $\Delta\tau_s$ and $\Delta\tau_e$ are the uncertainties in time due to straggling and systems noise respectively. Since τ, the time-of-flight can be expressed in terms of velocity or energy per nucleon, ε, of the ion,

$$\frac{\Delta\tau}{\tau} = K\,\varepsilon^{\frac{1}{2}}\,\Delta\tau_e\sqrt{1 + \left(\frac{\Delta\tau_s}{\Delta\tau_e}\right)^2}$$

where $K = (2/m_p)^{\frac{1}{2}}/S$, with m_p the proton rest mass and S the flight path. Since the systems noise is independent of the characteristics of the incident particle, $\Delta\tau_e$ should be constant. Indeed at higher energies where straggling is less important we observe an increase in $\Delta\tau/\tau$ with ε which is roughly consistent with $\Delta\tau/\tau \propto \varepsilon^{\frac{1}{2}}$. As ε decreases and straggling becomes significant the quantity in the square root becomes important. In spite of the scattering in the data points (resulting from systematic uncertainties in the foil thickness determination), the general trend represented by the shaded contour in Fig 5 shows that below ~30 keV/nucleon straggling becomes important and $\Delta\tau/\tau$ increases with decreasing velocity. If one takes the data point at 400 keV/nucleon as having an insignificant contribution due to energy straggling, (i.e., $\Delta\tau_s/\Delta\tau_e << 1$), then one obtains an estimate of the systems noise $\Delta\tau_e \sim 0.4$ ns. Taking this value of $\Delta\tau_e$, we estimate that $\Delta\tau/\tau \propto \varepsilon^{-0.7}$ at lower energies, which implies that the spread in velocity due to energy straggling in the foil is proportional to $\varepsilon^{-2/3}$. Although no real significance can yet be attached to this functional form, we point out that further refinement of our present technique can be useful in the study of straggling of low energy ions.

Stopping power: Results of four sets of measurements of the stopping power of various ion species in carbon foils are summarized in Fig 6. Set 1, (open symbols and *), was obtained by comparing the TOF measurements taken with and without an additional 9.8 $\mu g/cm^2$ foil in front of TOF-II. Similarly, Set 2, (half-filled H and He points), was taken by TOF-I using an additional 3.1 $\mu g/cm^2$ foil. Set 3, (solid symbols), was obtained by comparing the energy deposited in a solid-state detector taken with and without a 9.2 $\mu g/cm^2$ foil in front of the detector. Set 4, (half-filled nitrogen points), was taken in the same manner as Set 3, except the extra foil used is 2.6 $\mu g/cm^2$. Since the relative uncertainty in the foil thickness increases with decreasing thickness, especially

for <10 μg/cm^2 [5], we normalized all data sets to Set 1, (open symbols) by shifting these data points downward by an appropriate amount. The magnitudes of the downward shifts for the three sets of data are 65%, 75%, and 60% for Sets 2, 3 and 4 respectively, indicating that the errors in our stopping power measurements are primarily due to our poor knowledge of the foil thicknesses. The normalized results are compared with theoretical curves given by Northcliff and Schilling[6]. We note that although the theoretical curves (dashed) for Ar and N agree well with the respective experimental data, an upward shift by a factor of ∿1.4 seems necessary to bring the theoretical C, He and H curves into better agreement with our experimental results for these ions. The single measured Ne point, on the other hand, is well below the theoretical value. In general we note that in this energy range the total stopping power increases with increasing energy per nucleon as $\varepsilon^{\frac{1}{2}}$.

Charge states: An incident ion may have its charge state altered in passing through a thin foil due to interactions with the atomic electrons in the foil and with the electrons boiled off the surfaces of the foil. Inserting an additional carbon foil in front of TOF-I and having the added foil at a potential different from that at the entrance or START foil of TOF-I, we were able to identity the various charge states of the H and He emerging from the added front foil. The potential difference between the added foil and the entrance detector of TOF-I accelerates the emerging ions in proportion to their charge; therefore, ions of different charge states arrive at the start detector of TOF-I with correspondingly different energies and have different flight times.

The dash histograms in Figs. 7a and 7b represent the TOF signals of H^+ and He^+ respectively incident on TOF-I, without the additional foil, while the solid histograms correspond to the TOF distribution of these ions after traversing an additional 3.1 μg/cm^2 carbon foil placed in front of TOF-I. The

difference in the mean TOF between adjacent charge states of H and He corresponds to a 3.6 keV energy differences, which is due to the 3.6 kV potential difference between the added foil and the entrance detector of TOF-I. The fractional difference in the TOF, $\delta\tau/\tau$ between adjacent charge states of a given ion decreases as the incident energy, E of that ion increases (e.g. compare the case of the 10 keV versus the 25 keV H shown in Fig 7a) as is expected since $\delta\tau/\tau = -\delta E/(2E)$ where δE is fixed at 3.6 keV and $\delta E << E$. At 50 keV, the TOFs of H and H^+ become inseparable, and we note that the spread in TOF for neutral H and He is wider than that for the +1 charge state. A detailed study on the TOF distributions for the different charge states should thus provide information on the amount of scattering and straggling in foils for ions emerging with different final charge states.

From data similar to those shown in Fig 7 we obtained the relative abundance of final charge states of H^+ and He^+ ions with incident energies between 10 and 50 keV. Our results are summarized in Fig 8. Despite the rather unfortunate absence of measurements between 30 and 50 keV, it is clear that below 30 keV a large fraction of the emerging ions are neutral.

4. APPLICATIONS

The results reported above suggest that TOF telescopes using 2-5 g/cm carbon foil in the START detector when combined with solid state detectors can be of general use in atomic and low energy nuclear physics. We also point out that the energy range of these devices can be extended downward by providing modest post acceleration to the incident ions before they enter the TOF telescopes.

An important area where these techniques are now being applied is space physics. Measurements of the charge states (including zero state) and the chemical and isotopic compositions of low energy particles (both charged and

neutral) originating in the galaxy, the sun, and accelerated in the interplanetary medium and the magnetospheres of the earth, Jupiter and other planets are of fundamental importance in (a) identifying their sources of origin, (b) characterizing regions in space in which the particles are confined and through which they propagate, and (c) providing essential information on mechanisms responsible for their acceleration. Instruments based on the time-of-flight technique described in this paper, combined with electrostatic deflection analysis, post acceleration and energy measurements by means of solid state detectors will fill significant gaps in our knowledge of the compositions of thermal ($\sim$1 keV/nuc) and suprathermal ($\sim$1 to 300 keV/nuc) ions and neutral atoms of solar, interplanetary, interstellar, cometary and magnetospheric origin. To illustrate this application of the TOF technique we describe below two possible configurations suitable for space instruments.

In situ Analysis of Neutrals in Interplanetary Space and Cometary Atmosphere. In situ analysis of the abundances of neutral atoms and molecules at flux levels between 10^5 and 10^{15} molecules $cm^{-2}sec^{-1}$ should be possible using an array of sharp needles to field-ionize a fraction of the incoming neutral flux for TOF analysis. The advantages of field-ionization and a preliminary report on details of this device can be found elsewhere[7]. Fig 9 (taken from Reference 7) is a sample spectrum obtained using a field-ionization tip array in front of TOF-I. The mass resolution of TOF-I as demonstrated in Figs 4 and 9 is sufficient for in situ analysis of interplanetary neutral H, He, C, N, and O. For cometary studies, molecular identification must be achieved in the presence of the effects of particle straggling in the foil. Work towards this goal is now underway.

Measurements of Thermal and Suprathermal Charged Particles in Space. By combining the time-of-flight measurements with electrostatic deflection analysis, post-acceleration and a determination of the residual energy of the ion, one can obtain detailed information concerning the charge-state, isotopic and elemental composition as well as energy spectra of charged particles in the energy range between a few hundred eV and a few MeV per charge. Since a discussion of these techniques has been given elsewhere[8], we describe here only the principle of operation of such an instrument whose schematic representation is shown in Fig. 10.

An incoming ion, characterized by its energy E, charge state Q and mass M enters a large area, multi-slit collimator which defines the entrance trajectory of the ion. The electrostatic deflection analyzer selects ions which have the same E/Q ratios and allows these ions to enter the post-acceleration region and the time-of-flight (TOF) system. The ratio of the slit width of the exit slit in the deflection system to the total deflection determines the energy resolution $\Delta E/E$ (typically 7%) of the analyzer. The E/Q value is varied systematically by stepping the deflection voltage, V_d in logarithmic increments.

The ions are post-accelerated through a potential drop V_a of typically 30 kV thereby gaining sufficient energy to trigger the solid state detector (energy threshold $\sim$15 keV) which measures their residual energy.

Following post-acceleration, ions enter the time-of-flight system which serves to measure their velocity. Two secondary electron detector assemblies (SEDAs) separated by a typical distance d = 10 cm are used as the START and STOP detectors. From the time-of-flight τ, (typically 20-100ns) between the START and STOP signals the velocity (d/τ) of the post-accelerated ions can be determined. The carbon foil is thin enough so that the energy of the post-accelerated ions passing through it is not significantly degraded. The stop

SEDA is identical to the start SEDA except that the surface gold layer of the solid state detector (which measures the residual energy of the ion) is used instead of the carbon foil to generate the secondary electrons.

The solid-state detector (which is also part of the STOP SEDA) measures E'_{pa} which is a known fraction $1/\alpha$ of the energy E_{pa} of the post-accelerated ion. Energy loss in the gold contact of the detector, as well as non-ionizing collisions (nuclear defect) in the solid state detector are responsible for reducing E_{pa} by $1/\alpha$[9,10].

These measurements can then be combined to yield separately the mass, charge, and energy of an ion, as follows: The energy per charge (E/Q) selected by the electrostatic deflection analyzer, the known post-acceleration voltage (V_a), and the measured velocity (d/τ) in the TOF system yield M/Q according to $M/Q = 2(V_a + E/Q)/(d/\tau)^2$. The measured energy after post-acceleration (E'_{pa}), and the measured velocity (d/τ) in the TOF system yield M according to $M = 2(E'_{pa} \cdot \alpha)/(d/\tau)^2$. The calculated M/Q and M yield Q. Finally, the energy per charge (E/Q) selected by the electrostatic deflection analyzer and the calculated Q yield the energy E prior to post-acceleration, according to $E = Q \cdot (E/Q)$.

We have calibrated the TOF-II configuration using Van de Graaff beams of ^{1}H, ^{3}He, ^{4}He, ^{12}C, ^{14}N, ^{16}O, ^{20}Na and ^{40}Ar. The results of these calibrations are given in Fig. 11. The curves represent the calculated response taking into account energy losses in the carbon foil and gold layer[6] and the nuclear defect in the solid state detectors[9,10].

5. CONCLUSION

We have described several aspects of a time-of-flight arrangement consisting of a thin carbon foil, a secondary electron accelerating grid and a pair of MCPs, and illustrated possible applications in atomic, low-energy nuclear and space physics. Our present work provides preliminary measurements of (a) the

stopping power, and energy straggling of low energy particles in carbon foils, and (b) the equilibrium charge states of H and He as a function of energy. Not reported here are studies on angular distribution of the ions emerging from thin foils, and on the effect of the foil on fast molecules. We intend to continue our pursuit of these problems.

ACKNOWLEDGEMENTS

We would like to express our gratitude to R.A. Lundgren, B.A. Lambird and J. Cain for their invaluable technical assistance in many phases of our work and to Stephen Brown of Goddard Space Flight Center for his dedicated service in providing us with the desirable ion beams. One of us (KCH) expresses his appreciation to J.J. L'Heureux for his assistance during our accelerator runs, J.D. Garcia for his contribution to our interpretation of the TOF data on charge states, C.Y. Fan for helpful discussions on experimental procedures, an to the Office of Vice President for Research, University of Arizona for the necessary assistance in this research. We are grateful to James O. Benham and Adolf Asam of ITT Electro-Optical Products Division for providing us with microchannel plates used in this work. This research was supported in part by NASA grants NGR 02-002-107 (Univ. of Arizona), NGR 21-002-224 and NGR 21-002-316 (Univ. of Maryland).

Figure Captions

Figure 1 Schematic diagram of the two time-of-flight telescopes. (a) time-of-flight measurement only, (b) time-of-flight and residual energy measurement.

Figure 2 Pulse-height distributions of signals from (a) the START detector and (b) the STOP detector of TOF-I. The pulses are large enough such that no additional amplification is required before the discriminators whose respective thresholds are indicated by the vertical dashed lines. The ratio of channel length to channel diameter for the MCP is 40.

Figure 3 Block diagram of the electronics used in both TOF configurations.

Figure 4 Timing resolution for 25 KeV (a) H^+ and He^+, and (b) C^+, O^+ and CO^+ in the TOF-I telescope.

Figure 5 Time-of-flight resolution, $\Delta\tau/\tau$, vs. incident energy per nucleon, ε for a number of ion species. The spread below several hundred keV/nucleon is most likely due to energy straggling in the carbon foil.

Figure 6 Measured total stopping power for various ions in carbon. See text for a discussion of symbols and curves.

Figure 7 TOF distributions showing the final charge states of (a) H^+ and (b) He^+ ions after passage through a 3.1 $\mu g/cm^2$ carbon foil. The dashed histograms are the distributions taken without the 3.1 $\mu g/cm^2$ additional foil.

Figure 8 Relative abundance of charge states as a function of incident energy for (a) H^+ and (b) He^+ after passage through a 3.1 $\mu g/cm^2$ carbon foil. Although at 50 KeV, the 3.6 KeV difference between the H^+ and H is not sufficient to resolve the two charge states, the average TOF for these ions when compared with those at lower energies indicates the predominance of the +1 state.

Figure 9 TOF spectrum obtained by using a field-ionization tip to provide the ions generated from an undetermined proportion of H_2, CH_4, H_2O and residual air in the vacuum chamber. The vertical scale has been expanded in the region of the higher mass peaks. Energy straggling plays a dominant role for the higher masses.

Figure 10 Schematic representation of the charge- mass and-energy spectrometer for studies of charged particles in space.

Figure 11 Measured response of the TOF-II telescope with a 10 cm flight path exposed to various accelerated ion beams. Notice the clear separation of the isotopes of ^3He and ^4He.

REFERENCES

1. W.F.W. Schneider, B. Kohlmeyer and R. Bock, Nucl. Instr. and Meth., 87, (1970) 253.

   G.W. Butler, A.M. Poskanzer and D.A. Landis, Nucl. Instr. and Meth., 89, (1970) 189.

2. E. Dietz, R. Bass, A. Reiter, U. Friedland and B. Hubert, Nucl. Instr. and Meth., 97, (1971) 581.

3. E. Dietz, J.V. Czarnecki, W. Patscher, W. Schafer and R. Bass, Nucl. Instr. and Meth., 108, (1973) 607.

4. F.S. Goulding and B.G. Harvey, Ann. Rev. Nucl. Sci., 25 (1975) 201; G. Gabor, W. Schimmerling, D. Greiner, F. Biesner, and P. Lindstrom, Nucl. Instr. and Meth., 130 (1975), 65.

5. J.O. Stoner, Jr., Private communication (1977).

6. L.C. Northcliffe and R.F. Schilling, Nucl. Data Tables A7 (1970).

7. K.C. Hsieh, C.Y. Fan and J.J. O'Heureux, 15th International Cosmic Ray Conference, Conference Papers, Vol. 9, 163 (Plovdiv, 1977).

8. G. Gloeckler, University of Maryland Technical Report TR 77-043 (unpublished 1977).

9. H.E. Schitt, Mat. Fys. Medd. Dan. Vid. Selsk, 3e, no. 9 (1966).

10. F.M. Ipavich, R.A. Lundgren, B.A. Lambird and G. Gloeckler, Nuc. Instr. and Meth., 154 (1978) 291.

(a) TOF - I

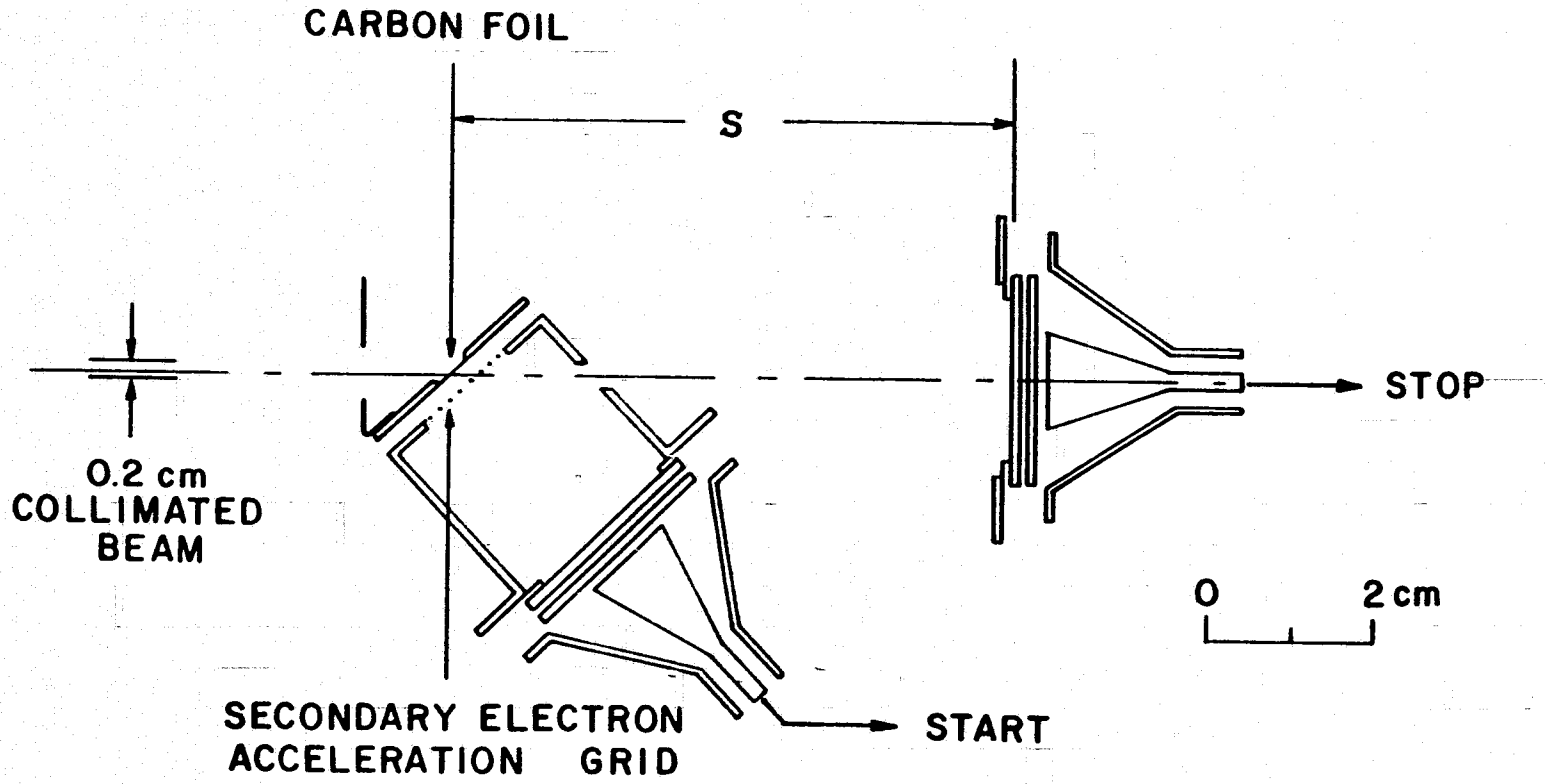
CARBON FOIL
S
STOP
0.2 cm
COLLIMATED
BEAM
0
2 cm
SECONDARY ELECTRON
ACCELERATION GRID
START

(b)

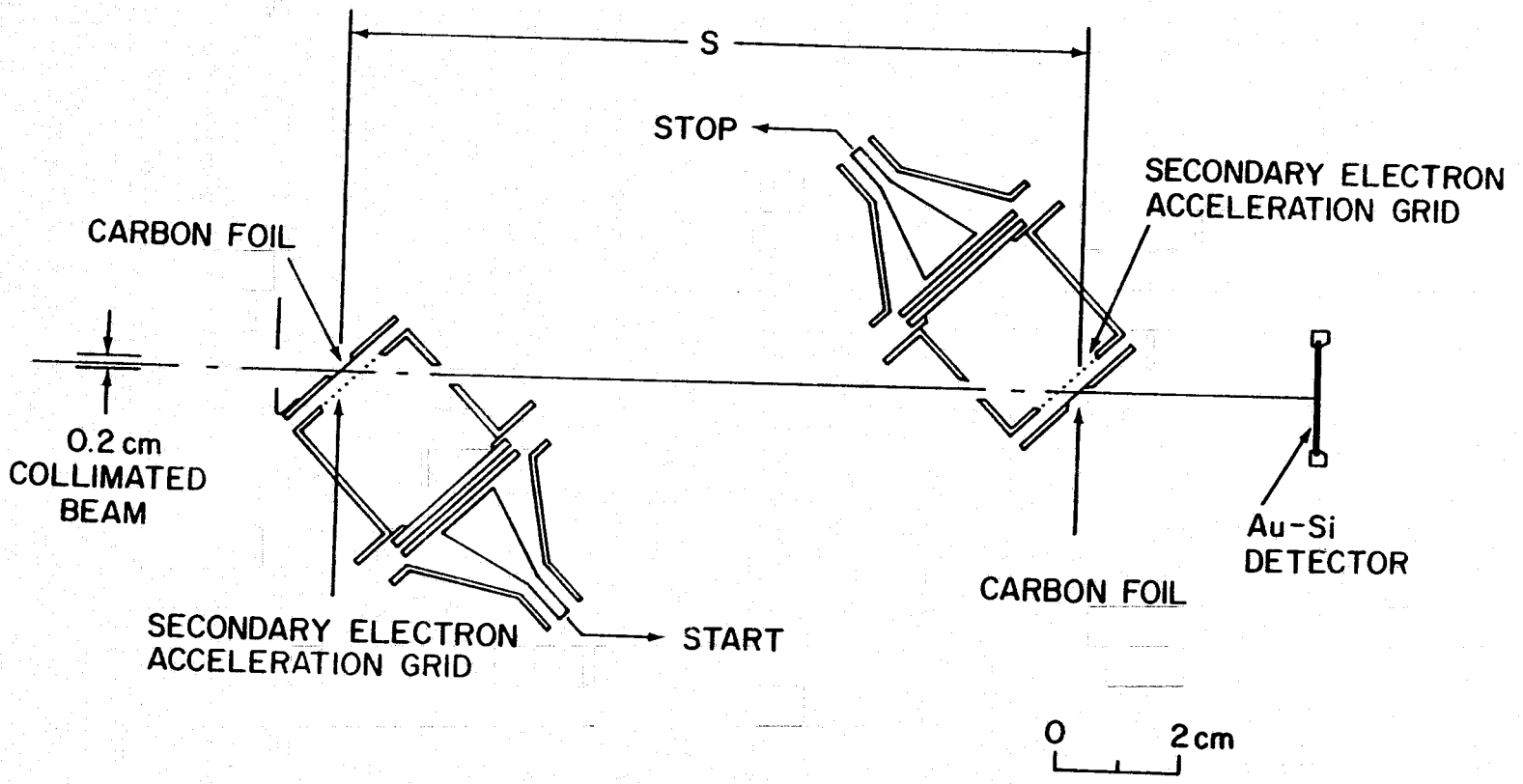
S
STOP
SECONDARY ELECTRON
ACCELERATION GRID
CARBON FOIL
0.2 cm
COLLIMATED
BEAM
Au-Si
DETECTOR
CARBON FOIL
SECONDARY ELECTRON
ACCELERATION GRID
START
0
2 cm

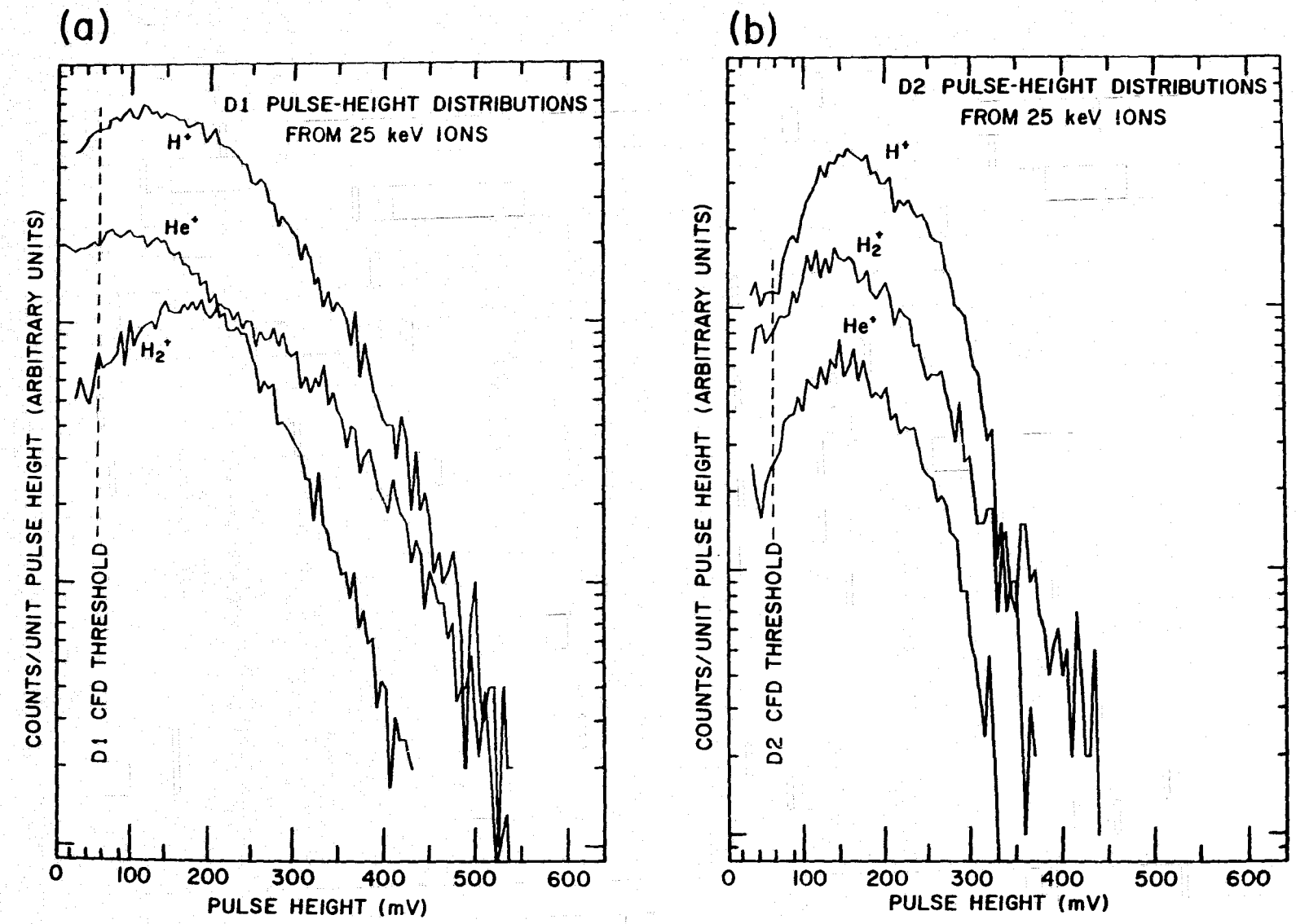
(a)
D1 PULSE-HEIGHT DISTRIBUTIONS
FROM 25 keV IONS
H+
He+
H2+
D1 CFD THRESHOLD
COUNTS/UNIT PULSE HEIGHT (ARBITRARY UNITS)
0
100
200
300
400
500
600
PULSE HEIGHT (mV)
(b)
D2 PULSE-HEIGHT DISTRIBUTIONS
FROM 25 keV IONS
H+
H2+
He+
D2 CFD THRESHOLD
COUNTS/UNIT PULSE HEIGHT (ARBITRARY UNITS)
0
100
200
300
400
500
600
PULSE HEIGHT (mV)

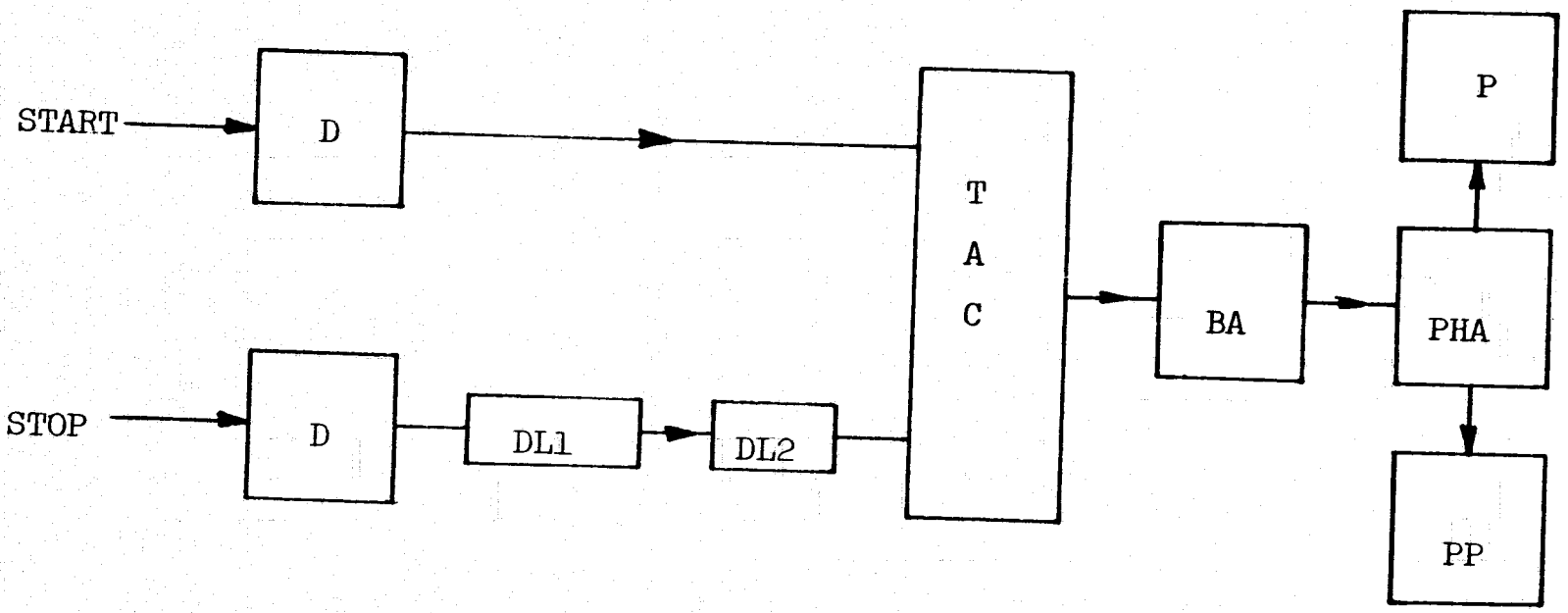

D = SNAP OFF discriminator

DL1 = fixed delay ∿ 150 ns

DL2 = calibrated delay 0-30 ns

TAC = time-to-amplitude converter

BA = biased amplifier

PHA = pulse-height analyzer

P = X-Y plotter

PP = paper-tape punch

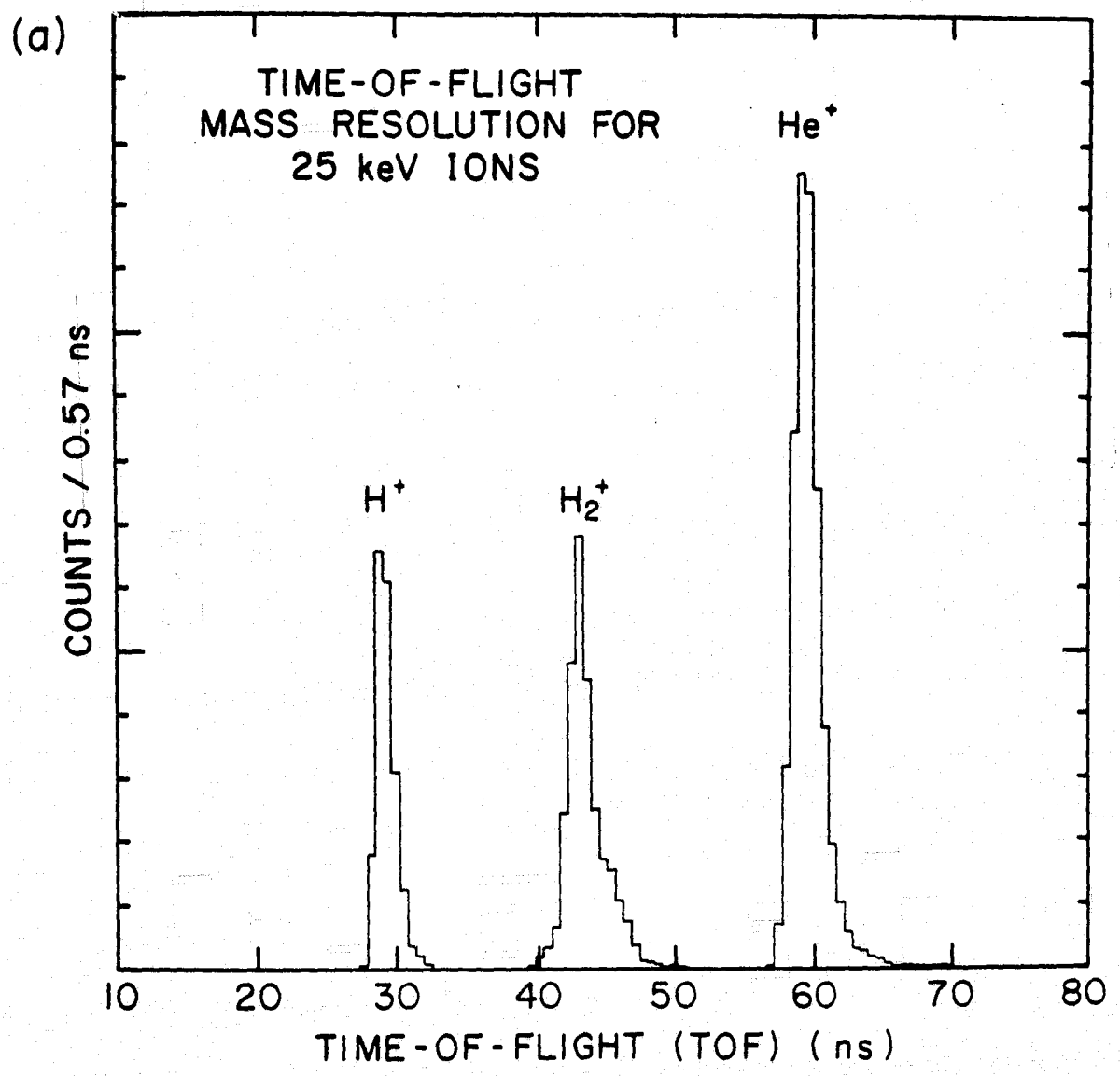
(a)
TIME-OF-FLIGHT
MASS RESOLUTION FOR
25 keV IONS
He+
H+
H2+
COUNTS / 0.57 ns
10
20
30
40
50
60
70
80
TIME-OF-FLIGHT (TOF) (ns)

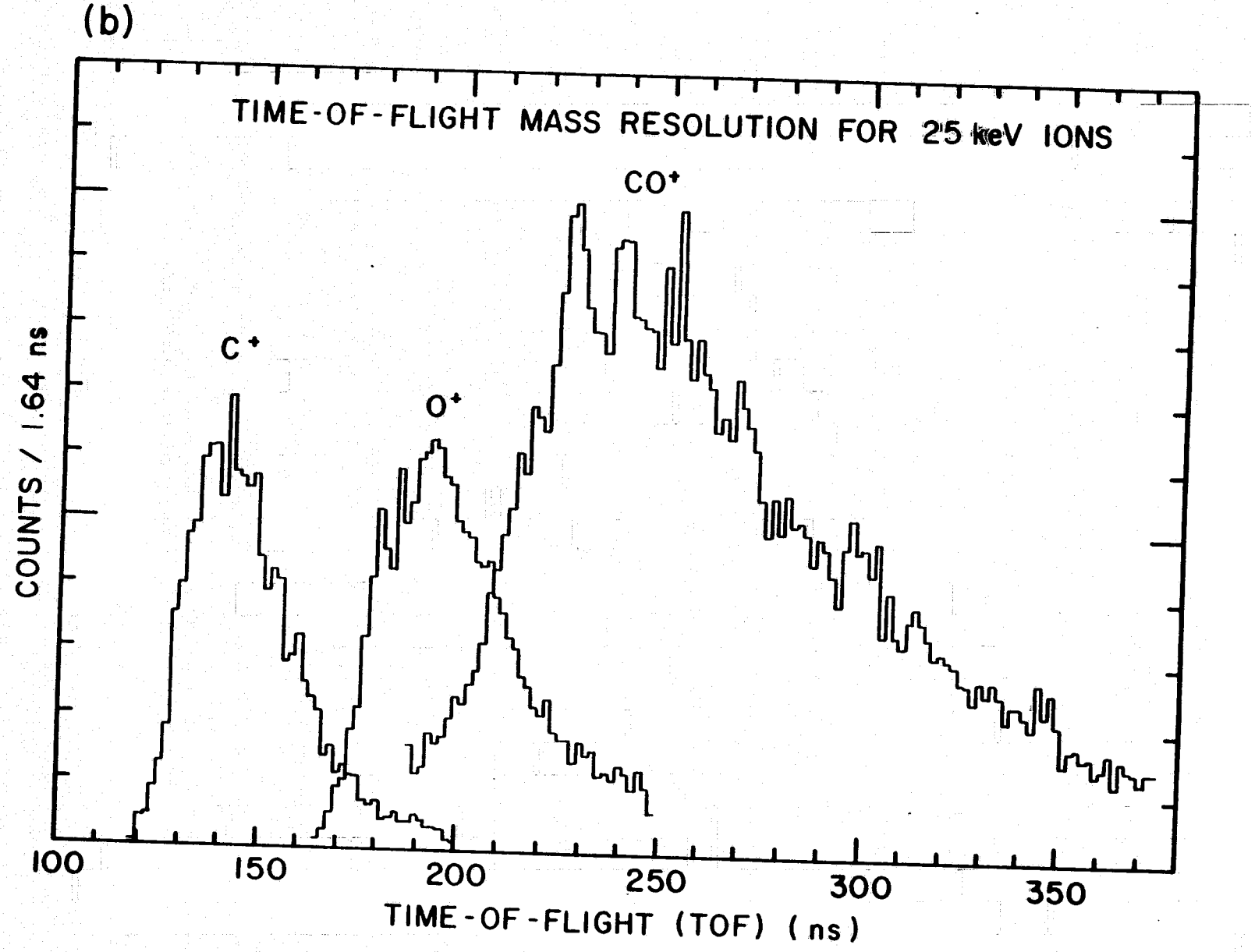
(b)
TIME-OF-FLIGHT MASS RESOLUTION FOR 25 keV IONS
CO+
C+
O+
COUNTS / 1.64 ns
100
150
200
250
300
350
TIME-OF-FLIGHT (TOF) (ns)

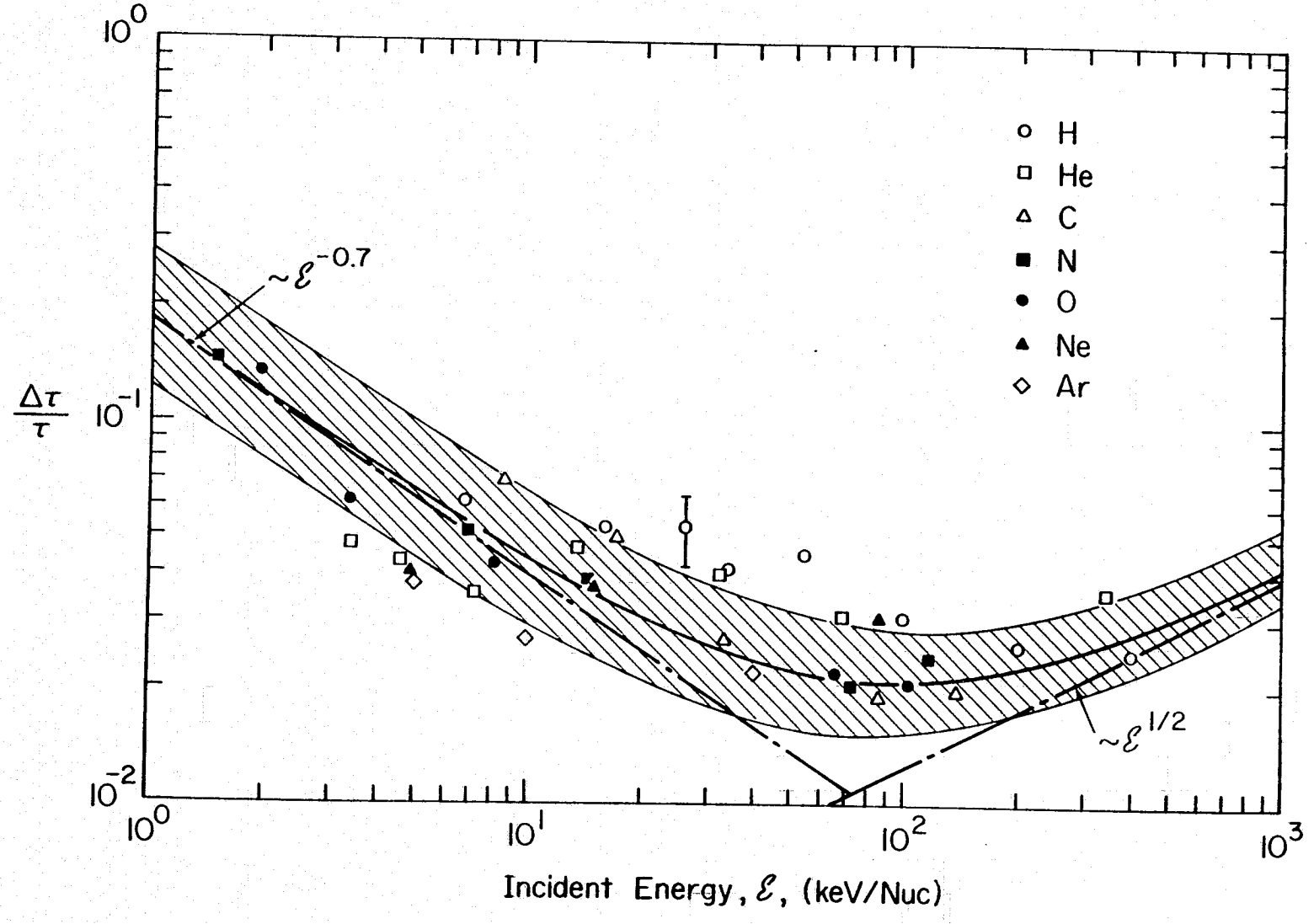
10^0
10^{-1}
10^{-2}
$\frac{\Delta\tau}{\tau}$
$\sim\mathcal{E}^{-0.7}$
$\sim\mathcal{E}^{1/2}$
H
He
C
N
O
Ne
Ar
10^0
10^1
10^2
10^3
Incident Energy, $\mathcal{E}$, (keV/Nuc)

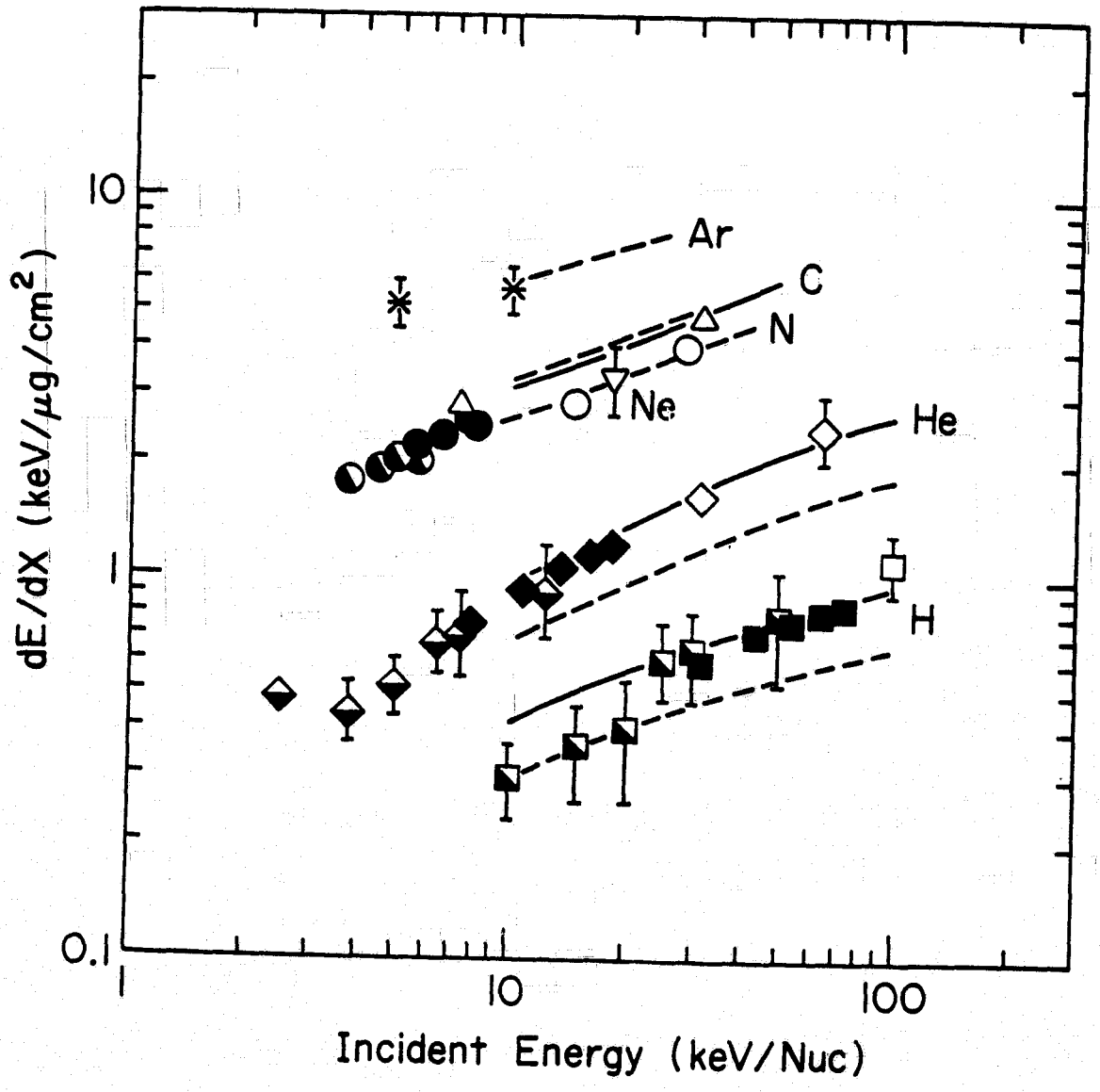
10
1
0.1
dE/dX (keV/μg/cm²)
Ar
C
N
Ne
He
H
1
10
100
Incident Energy (keV/Nuc)

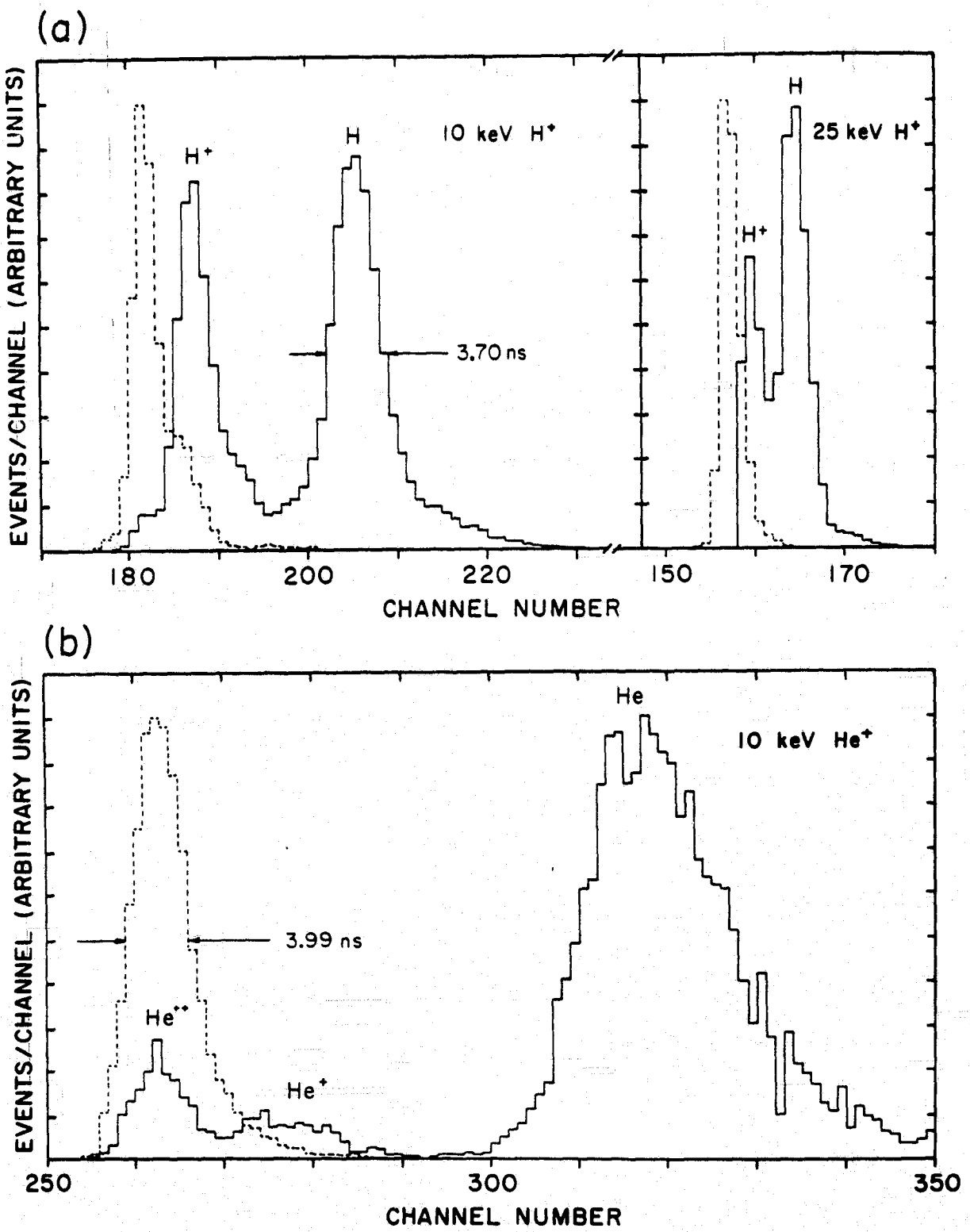
(a)
EVENTS/CHANNEL (ARBITRARY UNITS)
H+
H
10 keV H+
3.70 ns
H
H+
25 keV H+
180
200
220
150
170
CHANNEL NUMBER
(b)
EVENTS/CHANNEL (ARBITRARY UNITS)
He
10 keV He+
3.99 ns
He++
He+
250
300
350
CHANNEL NUMBER

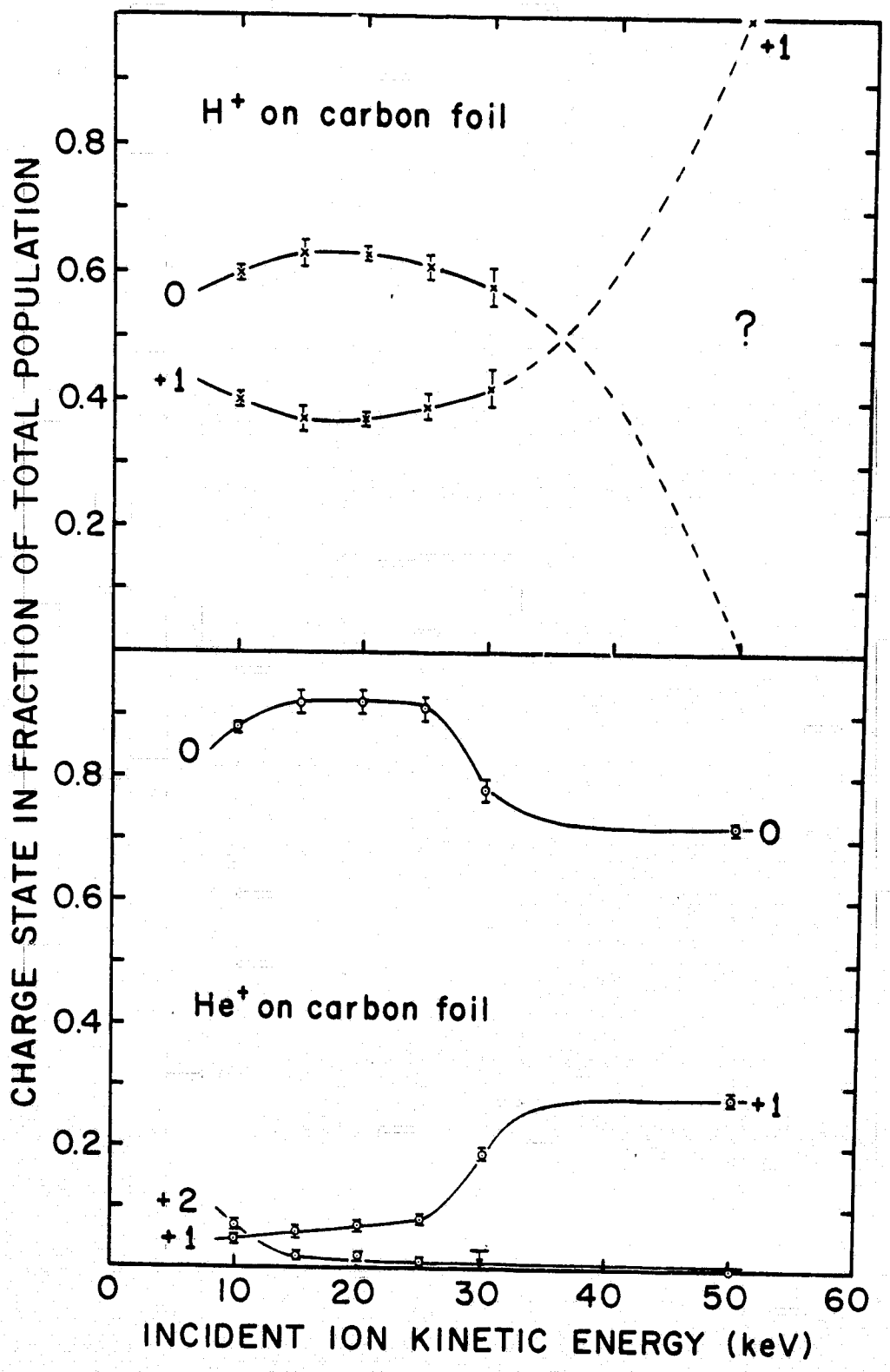
H+ on carbon foil
+1
0
+1
?
0.8
0.6
0.4
0.2
0
0.8
0.6
0.4
0.2
0
-0
He+ on carbon foil
-+1
+2
+1
0
10
20
30
40
50
60
CHARGE STATE IN FRACTION OF TOTAL POPULATION
INCIDENT ION KINETIC ENERGY (keV)

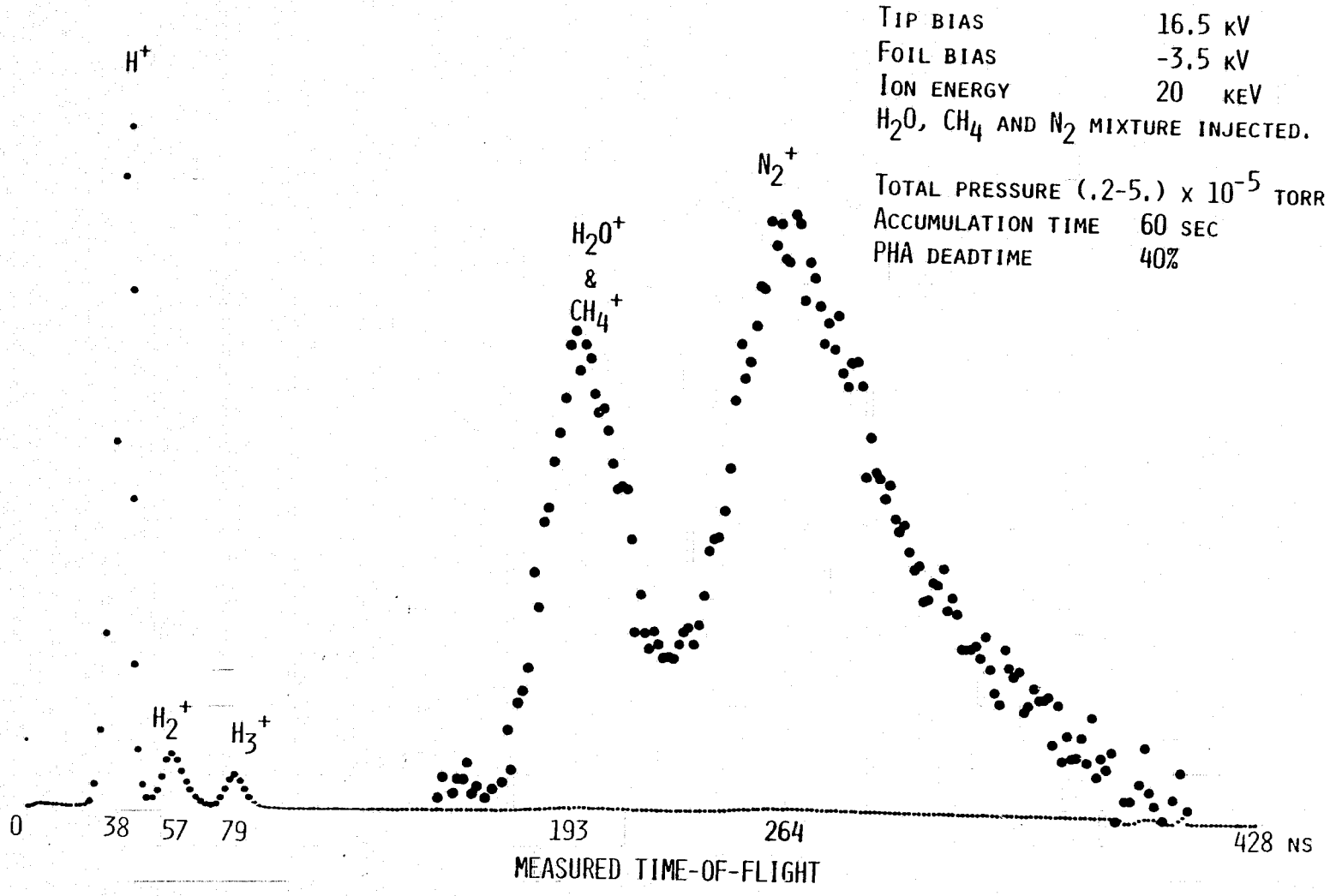
TIP BIAS 16.5 KV
FOIL BIAS -3.5 KV
ION ENERGY 20 KEV
H_2O, CH_4 AND N_2 MIXTURE INJECTED.
TOTAL PRESSURE (.2-5.) X 10^{-5} TORR
ACCUMULATION TIME 60 SEC
PHA DEADTIME 40%
H^+
H_2^+
H_3^+
H_2O^+
&
CH_4^+
N_2^+
0
38
57
79
193
264
428 NS
MEASURED TIME-OF-FLIGHT

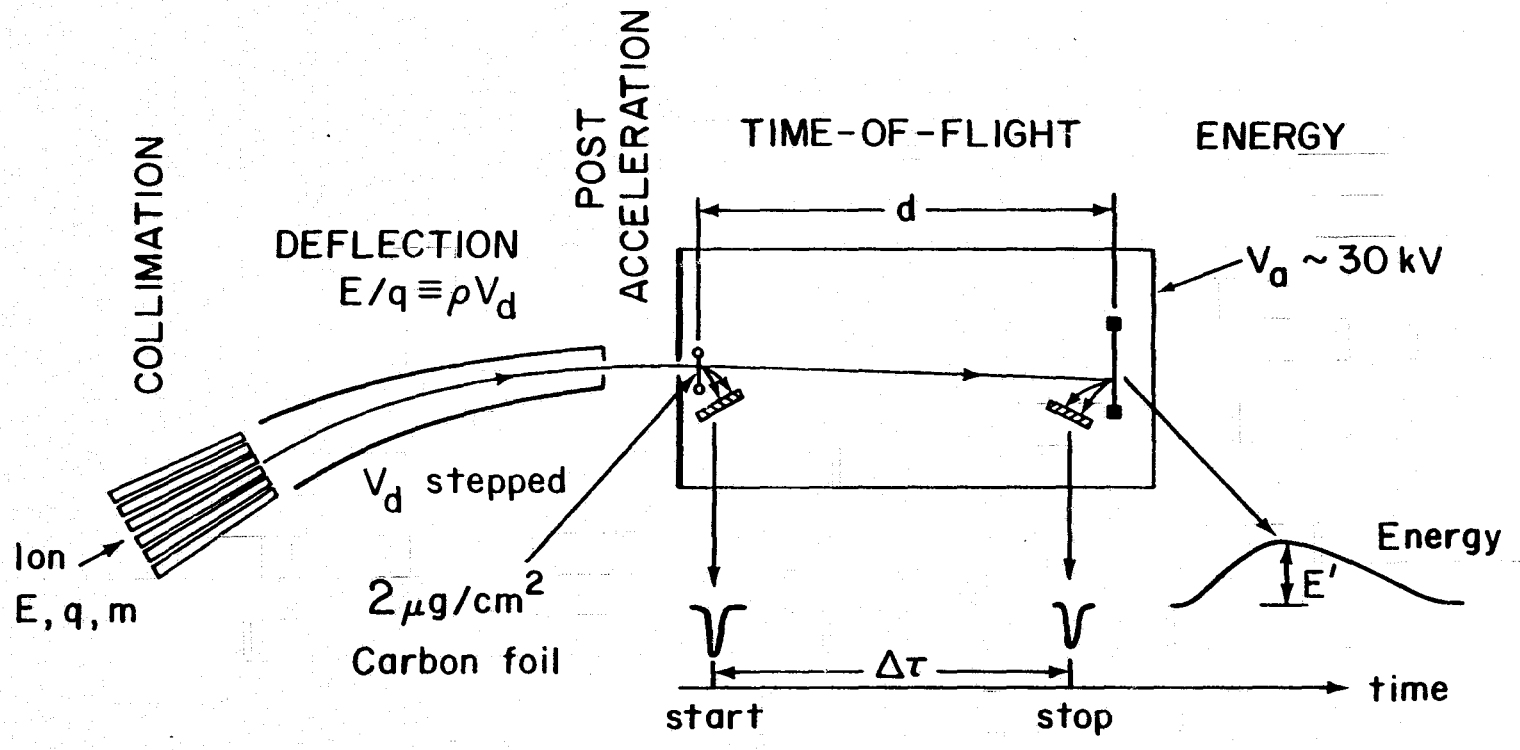
COLLIMATION
DEFLECTION
E/q ≡ ρV_d
POST
ACCELERATION
TIME-OF-FLIGHT
ENERGY
d
V_a ~ 30 kV
V_d stepped
Ion
E, q, m
2 μg/cm²
Carbon foil
Energy
E'
Δτ
start
stop
time

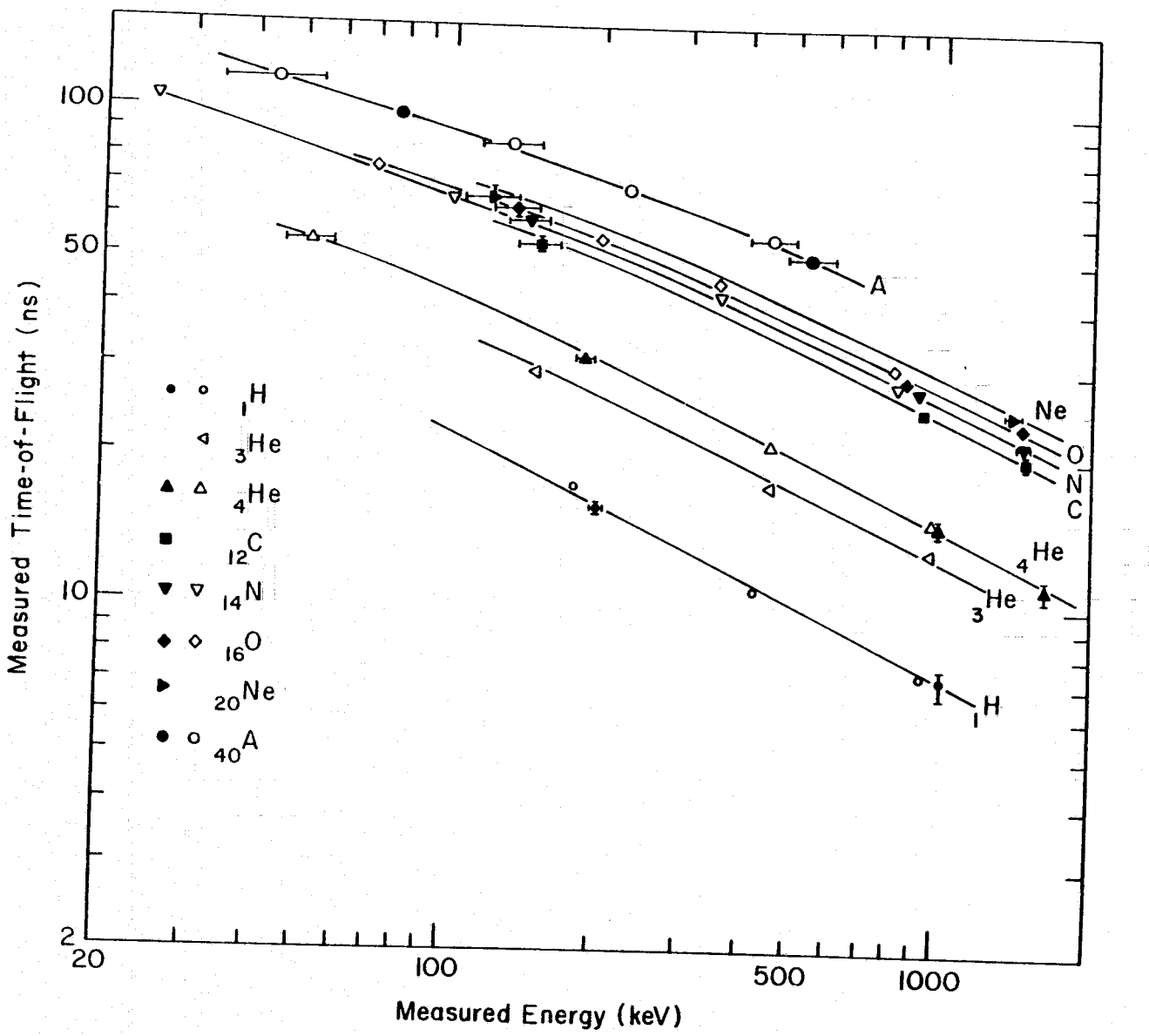
Measured Time-of-Flight (ns)
100
50
10
2
20
100
500
1000
Measured Energy (keV)
$_1H$
$_3He$
$_4He$
$_{12}C$
$_{14}N$
$_{16}O$
$_{20}Ne$
$_{40}A$
A
Ne
O
N
C
$_4He$
$_3He$
$_1H$